


**Short-range physics of the three-body recombination for ultracold helium atoms**Bin-Bin Wang <sup>\*</sup>*School of Physics and Astronomy, China West Normal University, Nanchong 637009, China*Yong-Chang Han *Department of Physics, Dalian University of Technology, Dalian 116024, China*

(Received 6 June 2023; accepted 20 November 2023; published 6 December 2023)

Generally, the three-body recombination (TBR) of the ultracold helium atoms in the zero-collision-energy limit could be described by the original zero-range (Efimov) universal function [E. Braaten, D. Kang, and L. Platter, *Phys. Rev. A* **75**, 052714 (2007)] using the scattering length  $a$  of the He-He interaction and a three-body parameter  $a_*$  as input, where  $a_*$  is associated with the positive scattering length at which an interference minimum in the TBR rate occurs at the threshold. This universal property has been reinvestigated by considering various post-Born-Oppenheimer (post-BO) effects on the relevant scattering process. It is found that a linear correction to  $1/a_*$  versus  $1/a$  should be introduced to give a better description of these considered TBR cases because of the finite-range effects. Particularly, such a correction may be ascribed not only to the general scattering properties associated with the Efimov channel at the short hyperradial distance, but also to the tunneling probability in the lowest incident channel. In addition, a successful fit of the modified universal function that includes correctly the finite-range effects [E. Garrido, M. Gattobigio, and A. Kievsky, *Phys. Rev. A* **88**, 032701 (2013)] or the zero-range universal function with a linearly variational  $1/a_*$  versus  $1/a$  to numerically accurate data also indicates a clear manifestation of the van der Waals universality. Finally, the post-BO effects on the TBR process for the partial wave with the total angular momentum  $J > 0$  are also discussed.

DOI: [10.1103/PhysRevA.108.062805](https://doi.org/10.1103/PhysRevA.108.062805)**I. INTRODUCTION**

Since the 1970s, it has been theoretically found that, when the  $s$ -wave scattering length  $a$  between any two components in a three-body system is much larger than its van der Waals length  $r_{\text{vdW}}$ , the ternary system has novel universal properties [1–4]. For instance, as  $a \rightarrow \pm\infty$ , i.e., in the unitary limit, an infinite sequence of weakly bound three-body states, which are called Efimov states and related to each other via a discrete scaling symmetry [1], will accumulate near the (three-body breakup) threshold. Since these states are so weakly bound, the scattering observables in the zero-collision-energy limit, i.e.,  $E \rightarrow 0$ , will be influenced by them and also exhibit similar universal properties [5]. Particularly, via the three-body recombination (TBR) process of the ultracold Cs atoms, i.e.,  $\text{Cs}+\text{Cs}+\text{Cs} \rightarrow \text{Cs}_2+\text{Cs}$ , the ground Efimov state has been successfully demonstrated for the first time in experiment [6], and the studies of the Efimov physics afterwards have been the focus in both experimental and theoretical investigations (see, e.g., Refs. [7–10] and references therein). In addition, except for extensive studies in the fields of traditional nuclear, atomic, and molecular physics, the three-body systems in the new research fields continue to be also found to exhibit such a universality (see, e.g., the Efimov effect in quantum magnets [11]).

Generally, in the Efimov scenario of the scattering observables, a three-body parameter (TBP)  $a_-$ , which is associated with the negative scattering length at which the threshold resonance of the first Efimov state occurs, is introduced to include all the effects of the detailed short-range interactions, and plays a critical role in fixing the whole Efimov spectra or the corresponding scattering observables [5]. Because the details of the short-range potentials are different in real systems,  $a_-$  has been long considered to have a nonuniversal character [5,12]. However, it has been found afterwards in ultracold gas experiments that the universal behavior of  $a_- \approx 10r_{\text{vdW}}$  is robust (within a 15% margin) near different broad Feshbach resonances for the same or different three-body systems (see, e.g., Refs. [13–15] and references therein).

Theoretically, the universality of the TBP  $a_-$  was first attributed to the quantum reflection [16] caused by the sharp drop of the three-body potential in the Efimov channel at short hyperradial distances. However, based on accurately numerical calculations using a number of two-body model potentials, Wang *et al.* showed that the Efimov channel does not exhibit a sharp drop, but a sharp repulsive wall at the small hyperradius  $R$  with  $R$  describing the size of the three-body system [17]. Particularly, it has been found that, when the number of the two-body bound states supported by the pairwise model potentials is large enough, the position of such a repulsive wall is converged to  $R \approx 2r_{\text{vdW}}$ , which prevents the reactants from getting much closer to experience the short-range interactions and consequently leads to the observed universal behavior of  $a_-$  in the experiments. Further investigations, also based on

<sup>\*</sup>Corresponding author: [binbinwang01@cwnu.edu.cn](mailto:binbinwang01@cwnu.edu.cn)

the model calculations, attribute the physical origin of such a repulsive wall to the three-body deformation caused by the two-body correlations [18].

Besides these model calculations, the  $^4\text{He}_3$  system, whose spectra and scattering properties can be calculated accurately, has long been viewed as one of the most typical real systems in exploring the Efimov physics [19–21]. In the framework of the effective field theory, Braaten and Hammer [22] calculated the TBR rate of the  $^4\text{He}_3$  system, whose excited state has been debated for a long time [21], but has been recently detected as the Efimov state [23], for several previously developed He-He potentials. From the results, another TBP  $a_*$ , which is associated with the positive scattering length at which an interference minimum in the TBR rate occurs at the threshold, is extracted. Particularly, it is found that the TBR rates predicted by the zero-range (Efimov) universal function are relatively different when the scattering length  $a$  and the two-body energy length  $a_B$  of the He-He potential are used respectively as the two-body input. Here,  $a_B$  is associated with the binding energy  $E_2$  of the weakly bound helium dimer through the relation  $E_2 = \hbar^2/(ma_B^2)$  with  $m$  being the mass of the  $^4\text{He}$  atom [24]. In addition, it should be emphasized that the TBP is originally defined as the binding wave number  $\kappa_*$  of the reference trimer at the unitary limit with the binding energy of this trimer given as  $E_* = \hbar^2\kappa_*^2/m$  [5]. All the other three-body parameters that are defined as the observables associated with the Efimov physics, e.g., the aforementioned  $a_-$  and  $a_*$ , are closely related to  $\kappa_*$  (see, e.g., Refs. [5,25–27] for the definitions and relations of different TBPs). Therefore, the universal character of  $a_-$  also implies that  $\kappa_*$  and  $a_*$  may have also universal properties and this conjecture is confirmed in the theoretical investigations [17,26]. Nowadays, the universality of all these TBPs is collectively called the van der Waals universality [28–30].

In later investigations, Braaten *et al.* further pointed out that the TBR rate of the  $^4\text{He}_3$  system may be better predicted by the zero-range universal function if the TBP  $a_*$  is extracted using  $a_B$  as the two-body input [31]. In addition, based on the only numerically accurate TBR rate at that time, they also constrained the universal functions for the TBR in the nonzero temperature and applied them to the  $^{133}\text{Cs}$  atoms. Shepard then calculated the TBR rate of the  $^4\text{He}_3$  system for several previously developed He-He potentials by solving accurately the three-body Faddeev equation in momentum space [32]. Based on their results, the universal functions for TBR in the nonzero temperature are refined. Recently, to give a better description of the accurate TBR rate of the  $^4\text{He}_3$  system in the zero-collision-energy limit, Garrido *et al.* proposed a modified universal function, which carefully includes the finite-range corrections by making substitutions for  $a$  and  $\kappa_*$  in the zero-range universal function, i.e., replacing  $a$  and  $\kappa_*$  by  $a_B$  and  $\kappa_* + \Gamma/a$  respectively, where  $\Gamma$  is an empirical parameter [33].

From another viewpoint, the departure of the zero-range universal predictions from the calculated realistic TBR rates implies that the short-range physics is non-negligible in the  $^4\text{He}_3$  system. Therefore, when different He-He representations are adopted in the three-body calculations, a variational  $a_*$  will be extracted from the zero-range universal function using the calculated TBR rates and the corresponding

scattering lengths of the He-He interactions as input. Of course, it is worth emphasizing that although the zero-range universal functions associated with the TBR rate for both the positive and negative sides of the scattering length are derived in the zero-range condition [5], they are widely used in the experiments to fit the experimental data and extract the aforementioned TBPs  $a_*$  and  $a_-$  for the finite scattering length [6,25], which consequently leads to the extraordinary finding of the van der Waals universality (see, e.g., Refs. [13–15]). In this paper, we will also devote special attention to the dependence of  $a_*$  that is extracted based on the zero-range universal function on the short-range physics for the  $^4\text{He}_3$  system.

Using the currently most accurate He-He potential [34,35], the Efimov physics associated with the TBR process of the  $^4\text{He}_3$  system is reinvestigated in this paper. Here, by considering respectively various post-Born-Oppenheimer (post-BO) effects on the standard BO potential of the He-He interaction, a series of numerically accurate TBR rates are calculated, which permits us to give a rigorous check of the ability of the zero-range universal function in predicting the realistic TBR rates and study the possible variational behavior of the extracted  $a_*$  for the present cases. Particularly, the mechanisms underlying the relevant TBR process will be also analyzed. In addition, the present paper also gives an intuitive picture of the various post-BO effects on the TBR process and the numerically accurate results could be also used to modify the universal functions for TBR in the nonzero temperature. Atomic units are used throughout this paper except explicitly stated otherwise.

## II. THEORETICAL APPROACH

### A. The adiabatic hyperspherical method

To obtain the accurate TBR rate, the three-body Schrödinger equation is solved numerically using the adiabatic hyperspherical method. Since this method has been detailed in our previous work [36], only the outline is given in this paper. In the adiabatic hyperspherical representation [37], the channel functions  $\{\psi_\nu(R; \Omega)\}$ , and the corresponding eigenvalues  $\{U_\nu(R)\}$  are obtained via solving the hyperangular eigenvalue problems for a series of fixed  $R$ :

$$\left[ \frac{\Lambda^2}{2\mu R^2} + \frac{15}{8\mu R^2} + V(R, \theta, \varphi) \right] \Phi_\nu(R; \Omega) = U_\nu(R) \Phi_\nu(R; \Omega), \quad (1)$$

where  $\Omega$  denotes collectively the hyperangular coordinates, including three external Euler angles  $(\alpha, \beta, \gamma)$  and two internal hyperangles  $(\theta, \varphi)$ .  $\mu$  is the three-body reduced mass and  $\Lambda^2$  is the grand angular momentum operator.  $V(R, \theta, \varphi)$  is the three-body interaction. Here, for comparison with the model calculations [17,18,27], this interaction is also taken as a sum of three pairwise interaction potentials, i.e., three He-He potentials, in this paper. The effect of the nonadditional three-body force on the TBR process of the  $^4\text{He}_3$  system is found to be vanishingly small (see Ref. [38]).

After solving the adiabatic hyperangular eigenvalue problem, i.e., Eq. (1), the three-body wave function can be

expanded on these obtained channel functions  $\{\Phi_\nu\}$ :

$$\psi(R, \Omega) = \sum_{\nu=1}^N \zeta_\nu(R) \Phi_\nu(R; \Omega), \quad (2)$$

where  $\zeta_\nu(R)$  denotes the radial wave functions and  $N$  denotes the number of the total adopted channels.

Then, inserting this expansion into the original Schrödinger equation, we will get a set of coupled equations associated with the hyperradial part [37]:

$$\begin{aligned} & \left[ -\frac{1}{2\mu} \frac{d^2}{dR^2} + W_\nu(R) \right] \zeta_\nu(R) \\ & - \frac{1}{2\mu} \sum_{\nu' \neq \nu} \left[ 2P_{\nu\nu'}(R) \frac{d}{dR} + Q_{\nu\nu'}(R) \right] \zeta_{\nu'}(R) \\ & = E \zeta_\nu(R), \end{aligned} \quad (3)$$

with

$$W_\nu(R) = U_\nu(R) - \frac{Q_{\nu\nu}(R)}{2\mu}, \quad (4)$$

$$P_{\nu\nu'}(R) = \left\langle \Phi_\nu(R; \Omega) \left| \frac{\partial}{\partial R} \right| \Phi_{\nu'}(R; \Omega) \right\rangle_\Omega, \quad (5)$$

$$Q_{\nu\nu'}(R) = \left\langle \Phi_\nu(R; \Omega) \left| \frac{\partial^2}{\partial R^2} \right| \Phi_{\nu'}(R; \Omega) \right\rangle_\Omega$$

where  $W_\nu(R)$  denotes the effective three-body potentials, and  $P_{\nu\nu'}(R)$  and  $Q_{\nu\nu'}(R)$  are the nonadiabatic couplings that are responsible for the TBR process. The subscript  $\Omega$  denotes that only the integral over the hyperangular coordinates is performed. In addition, to trace the pathway of the flow in the TBR process, the nonadiabatic coupling strengths are also calculated [36]:

$$F_{\nu\nu'}(R) = \frac{|P_{\nu\nu'}(R)|^2}{2\mu |W_{\nu'}(R) - W_\nu(R)|}. \quad (6)$$

Finally, Eq. (3) is solved using the  $\mathcal{R}$ -matrix propagation method [39], and the  $\mathcal{S}$  matrix is obtained from the calculated  $\mathcal{R}$  matrix. The TBR rate is then directly associated with the  $\mathcal{S}$  matrix [37]:

$$K_3 = \sum_i \frac{192\pi^2}{\mu k^4} |S_{f \leftarrow i}|^2, \quad (7)$$

with  $k = \sqrt{2\mu E}$  being the hyperradial wave number.  $i$  and  $f$  indicate the incident and recombination channels, respectively. For the  ${}^4\text{He}_3$  system, there is only one recombination channel, which corresponds to the so-called Efimov channel [17,18] and is associated with the weakly bound  ${}^4\text{He}_2$  molecule, i.e.,  ${}^4\text{He}_2 + {}^4\text{He}$ .

### B. The post-BO effects and scattering properties of the He-He interactions

For the He-He interaction, a very accurate representation was constructed by Przybytek *et al.* [34] and Cencek *et al.* [35], which includes various post-BO contributions to the standard BO potential  $V_B(r)$ . The major post-BO effects are, namely, the adiabatic corrections [here denoted as  $V_A(r)$ ] originating from the coupling of the electronic and

nuclear motions, the relativistic effects to the Schrödinger equation [ $V_R(r)$ ], the quantum electrodynamics corrections [ $V_Q(r)$ ], and the Casimir-Polder retardation effects [ $V_{r.c.}(r)$ ] [40] (see also Figs. 5 and 6 in Ref. [35] for these post-BO effects).

Here, to get a series of numerically accurate TBR rates, these post-BO effects have been carefully readded into the standard BO potential. The energy differences between  $V_B(r)$  and our reconstructed ones, as well as two widely adopted He-He potentials, i.e., the LM2M2 [41] and HFD-B3-FCI1 He-He potentials [42], are shown in Fig. 1(a). As shown in this figure, the major differences of these potentials are located at a short internuclear distance [see also the inset of Fig. 1(a), which provides the opportunity to assess these two-body short-range effects on the three-body process]. Note that because of the cancellation of some post-BO effects, most of the variational properties shown in the inset of Fig. 1(a) are different from those of the individual post-BO contributions discussed in Ref. [35]. In addition, in this figure, the standard BO potential and these post-BO effects are concisely denoted by the subscripts attached to their contributions, e.g., “B” stands for  $V_B(r)$  and “A” denotes  $V_A(r)$ . Putting these labels together means the sum of the relevant interactions or corrections. For instance, “BA” denotes that the He-He potential is constructed by  $V_B(r) + V_A(r)$ . We also use such labeling rules in the following tables and figures to denote the adopted He-He potentials in the three-body calculations.

The corresponding two-body binding energies and scattering properties of these reconstructed He-He potentials as well as the two widely adopted He-He potentials are shown in Table I. As can be seen, because the scattering length of the He-He interaction is much larger than its corresponding van der Waals length, a very weakly bound state appears and varies versus the scattering lengths of different He-He representations. However, since the scattering lengths of these He-He potentials are not anomalously large, the scattering properties shown in Table I may not be well described by the two-body universal functions that are derived at the unitary limit [43]. For instance, although the variation of the scattering length  $a$  of the He-He interaction follows that of the corresponding two-body energy length  $a_B$  [22,43], the difference between them still exists. Actually, based on the effective field theory approach, a modified two-body universal function associated with the relation of  $a$  and  $a_B$  is derived, which gives [24]

$$\frac{r_e}{a_B} = \frac{r_e}{a} + \frac{1}{2} \frac{r_e^2}{a_B^2}. \quad (8)$$

Here,  $r_e$  is the effective range. As shown in Fig. 1(b), with such a modified two-body universal function, the numerical data associated with  $a$  and  $a_B$  of the He-He potentials could be well reproduced.

### C. Computational details

In the calculations, the lowest 20 channels are used and, by designing the bases in the hyperangular coordinates carefully,  $U_\nu(R)$  is calculated to be converged to at least eight digits for all the cases considered in this paper. In the hyperradial part, 320 finite element sectors are used in the region of the

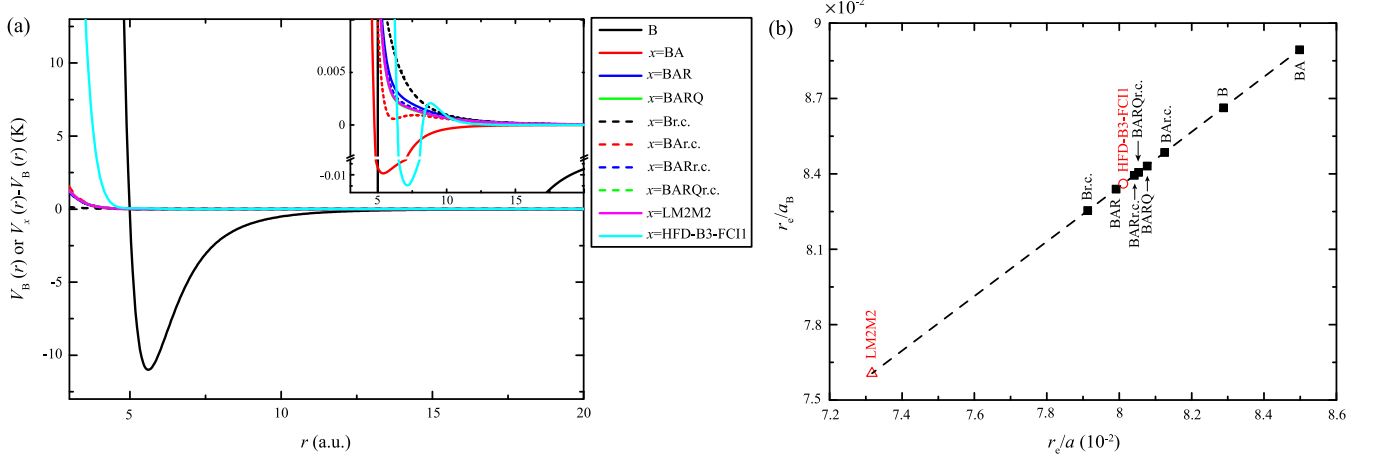


FIG. 1. (a) The Born-Oppenheimer representation of the He-He interaction,  $V_B(r)$ , and the energy differences between  $V_B(r)$  and our constructed He-He potentials. The differences between  $V_B(r)$  and the two widely adopted He-He potentials, i.e., the LM2M2 [41] and HFD-B3-FCI1 [42] potentials, are also shown. The inset zooms in on these differences. (b) The variation of the inverse of the two-body energy length  $a_B$  vs the inverse of the scattering length  $a$  for different He-He interactions (symbols), shown in units of  $r_e$ . The dashed line is given by Eq. (8).

short hyperradial distance ( $R < 2.5 \times 10^3$  a.u.), while 10 000 sectors are used in the large- $R$  region ( $2.5 \times 10^3 \leq R \leq 6 \times 10^5$  a.u.). In addition, we used ten points within each sector. Under such settings, the numerical results about the TBR rates are checked to be converged to three digits.

### III. RESULTS AND DISCUSSIONS

In the framework of universal theories, when the scattering length  $a$  is positive and much larger than its relevant van der Waals length  $r_{\text{vdW}}$ , a universal function for the TBR, leading to the formation of weakly bound products, has been derived based on the zero-range model at  $E \rightarrow 0$  [5,31]:

$$K_3 = \frac{768\pi^2(4\pi - 3\sqrt{3}) \sin^2[s_0 \ln(a/a_*)] a^4}{\sinh^2(\pi s_0) + \cos^2[s_0 \ln(a/a_*)] m}, \quad (9)$$

where  $s_0$  is roughly 1.006 24 for three identical bosons. Note that based on the relation  $a_* = e^{-1.16/s_0}/\kappa_* \approx 0.32/\kappa_*$  [5], the zero-range universal function, i.e., Eq. (9), could be

transformed to another well-known form containing the TBP  $\kappa_*$  [see also Eq. (11)]. Additionally, for real systems close to the unitary point, the zero-range model is merely an approximation, and there are always finite-range corrections, even in the unitary limit.

In the following discussions, it will be clearly found that the presence of a finite range in the real potential undermines the validity of the zero-range universal function. There are several ways to take this fact into account, and two of them could be actually identified from Sec. I. One is considering carefully the finite-range effects by introducing appropriate modifications of the zero-range universal function [see also Eq. (10) and the relevant discussions]. The other one is encapsulating directly the short-range physics or the finite-range effects in the TBP  $a_*$  of Eq. (9). As emphasized in Sec. I, if Eq. (9) is still adopted to describe the scattering process of the real systems with the finite scattering length and the correction of the short-range physics is negligible or identical for different systems, a universal  $a_*$  could be extracted [13–15].

TABLE I. Two-body binding energies  $E_2$ ,  $s$ -wave scattering lengths  $a$ , two-body energy lengths  $a_B$ , effective ranges  $r_e$ , and the van der Waals lengths  $r_{\text{vdW}}$  for different He-He potentials. The first eight rows show these associated with the reconstructed He-He potentials [34,35]. The remaining two rows display those calculated with the LM2M2 [41] and HFD-B3-FCI1 [42] potentials. The two-body energy length  $a_B$  is related to  $E_2$  through  $E_2 = \hbar^2/(ma_B^2)$  with  $m$  being the mass of the  $^4\text{He}$  atom and  $r_{\text{vdW}} = (mC_6/\hbar^2)^{1/4}/2$  [43]. The conversion constant  $\hbar^2/m = 12.119\,358$  K  $\text{\AA}^2$ .

Potential	$E_2$ (a.u.)	$E_2$ (mK)	$a$ (a.u.)	$a$ ( $\text{\AA}$ )	$a_B$ (a.u.)	$a_B$ ( $\text{\AA}$ )	$r_e$ (a.u.)	$r_e$ ( $\text{\AA}$ )	$r_{\text{vdW}}$ (a.u.)	$r_{\text{vdW}}$ ( $\text{\AA}$ )
B	$5.441 \times 10^{-9}$	1.718	165.898	87.789	158.715	83.988	13.75	7.28	5.081	2.689
BA	$5.751 \times 10^{-9}$	1.816	161.559	85.494	154.378	81.693	13.73	7.27		
BAR	$5.034 \times 10^{-9}$	1.590	172.182	91.115	165.004	87.316	13.76	7.28		
BARQ	$5.130 \times 10^{-9}$	1.620	170.605	90.280	163.446	86.492	13.78	7.29		
Br.c.	$4.924 \times 10^{-9}$	1.555	174.019	92.087	166.838	88.287	13.77	7.29		
BAr.c.	$5.219 \times 10^{-9}$	1.648	169.228	89.551	162.048	85.752	13.75	7.28		
BARr.c.	$5.100 \times 10^{-9}$	1.611	171.110	90.547	163.930	86.748	13.76	7.28		
BARQr.c.	$5.115 \times 10^{-9}$	1.615	170.864	90.417	163.684	86.618	13.76	7.28		
LM2M2	$4.140 \times 10^{-9}$	1.307	189.150	100.094	181.956	96.287	13.84	7.33	4.983	2.637
HFD-B3-FCI1	$5.045 \times 10^{-9}$	1.593	172.009	91.023	164.822	87.220	13.78	7.29	4.978	2.634

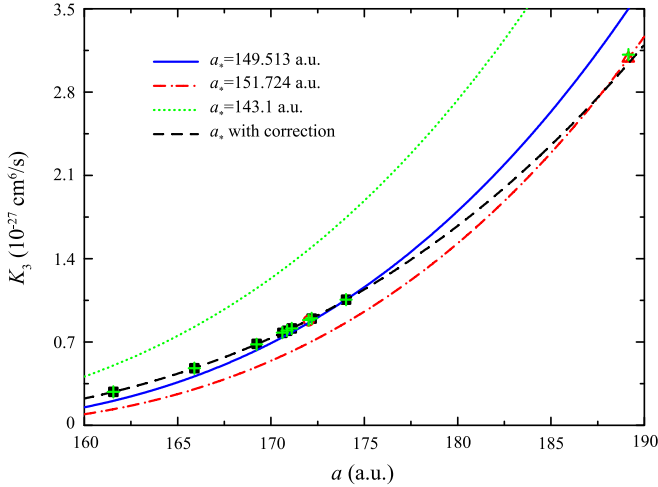


FIG. 2. The recombination rates  $K_3$  predicted by the zero-range universal function (curves) with different three-body parameters  $a_*$  [see Eq. (9)], by the modified universal function (plus symbols) with the fitted parameters  $\kappa_* = 1.906 \times 10^{-3}$  a.u. and  $\Gamma = 4.086 \times 10^{-2}$  a.u. [see Eq. (10)], and numerically calculated using different He-He potentials (other symbols). The black dashed curve denotes that  $K_3$  is calculated by the zero-range universal function Eq. (9), but with  $a_*$  being corrected (see Fig. 3).

In contrast, a varying  $a_*$  implies that the short-range dynamics plays a non-negligible role in the scattering process.

Since  $a$  of the He-He interaction is much larger than its  $r_{\text{vdW}}$  (see Table I), the present  ${}^4\text{He}_3$  system has long been considered to have the feature of the Efimov physics and its TBR rate should follow the zero-range universal function Eq. (9) [22,31]. To seriously check the ability of Eq. (9) in predicting the TBR process of the  ${}^4\text{He}_3$  system, a series of TBR rates, based on various He-He potentials shown in Table I, are calculated and shown versus  $a$  of the He-He potentials in Fig. 2. Based on the construction rule of these reconstructed He-He interactions and the data shown in this figure and Table I, each post-BO effect on the TBR process can be easily identified. Here, it is interesting to note that no matter how different the short-range He-He potentials are [see the inset of Fig. 1(a)], the TBR rates of all these cases are likely to be only determined by  $a$  of the He-He interactions. In the following, we will discuss whether the variation of these accurate TBR rates versus  $a$  of the He-He potentials could be well predicted by the zero-range universal function. Because a larger  $a$  corresponds to a smaller effect of the short-range physics on the low-energy scattering process, the TBR rate associated with the largest  $a$  among these reconstructed He-He potentials (see the last black square in Fig. 2) is first used to extract  $a_*$  of Eq. (9). This gives  $a_* = 149.513$  a.u. and the corresponding prediction about the variation of the TBR rate is shown as the blue solid curve in Fig. 2. As can be seen, with the decrease of  $a$ , the prediction of Eq. (9) tends to gradually deviate from and underestimate the numerically accurate TBR rates. Of course, when  $a_*$  is extracted using the TBR rate associated with the case of the largest  $a$  (red open triangle) as the three-body input, such a deviation between the predictions of the zero-range universal function (red dashed-dotted curve) and the accurate TBR rates also appears as the decrease of  $a$ .

This implies that the corrections of the finite-range effects or the short-range physics are non-negligible in the TBR process of the  ${}^4\text{He}_3$  system, and modifications of the zero-range universal function should be required to incorporate such corrections. In Ref. [31], it was suggested that a better prediction could be made by Eq. (9) when  $a_*$  is extracted using  $a_B$  instead of  $a$  as the two-body input. Based on the only numerically accurate TBR rate at that time, i.e., the one calculated with the HFD-B3-FC11 He-He potential (see the red open circle in Fig. 2), and the relevant  $a_B$  (see Table I), they obtained  $a_* = 143.1$  a.u. The prediction of Eq. (9) with this value of  $a_*$  is also displayed in Fig. 2 (see the green dotted curve), which, unfortunately, tends to be even worse. To give a much better description of the accurate TBR rates, more modifications to the zero-range universal function were proposed by Garrido *et al.* [33], which then includes correctly the finite-range corrections and gives [44]

$$K_3 = \frac{768\pi^2(4\pi - 3\sqrt{3}) \sin^2[s_0 \ln(a\kappa_* + \Gamma) + 1.16] a_B^4}{\sinh^2(\pi s_0) + \cos^2[s_0 \ln(a\kappa_* + \Gamma) + 1.16]} \frac{a_B^4}{m}. \quad (10)$$

Note that, as introduced in Sec. I, Eq. (10) is actually obtained by replacing  $a$  (associated with the  $a^4$  scaling) and  $\kappa_*$  in the zero-range universal function containing  $\kappa_*$  [see Eqs. (9) and (11)] by  $a_B$  and  $\kappa_* + \Gamma/a$ , respectively. Here, the  $K_3$ , calculated using the reconstructed He-He potentials associated with the smallest and largest  $a$  (the first and last black squares in Fig. 2), and the corresponding  $a_B$  (see Table I) are used as input to extract the parameters  $\kappa_*$  and  $\Gamma$  in Eq. (10), which consequently gives  $\kappa_* = 1.906 \times 10^{-3}$  a.u. and  $\Gamma = 4.086 \times 10^{-2}$  a.u. Based on these fitted parameters, it is found that the predictions of this modified universal function agree with the numerically accurate TBR rates very well (see the plus and other symbols in Fig. 2).

Using the fitted  $\kappa_*$ , the corresponding binding energy of the reference trimer at the unitary limit is determined to be  $E_* \approx 0.16$  mK, which is 519 times smaller than that of the reference trimer associated with the ground state of the  ${}^4\text{He}_3$  system [45] and clearly associated with the excited (Efimov) state. Interestingly, although the structure of the ground helium trimer does not satisfy fully the properties of the Efimov states, the energy ratio of the aforementioned two reference trimers is close to the neighboring energy ratios of the Efimov states ( $\approx 515$ ). In addition, the perfect fit of Eq. (10) to our numerical data with such a single  $\kappa_*$  implies that the energy of the reference trimer at the unitary limit, or  $\kappa_*$ , remains independent of the interaction potentials under consideration. This universal property is similar to the well-known universality exhibited by different He-He potentials, which all yield a ground-state energy value at the unitary limit of  $E'_* = 83$  mK (see Ref. [45]). To further check this universality, the modified Efimov binding-energy equation proposed by Kievsky and Gattobigio [see Eq. (7) of Ref. [46]] is employed to fit the energies of the helium excited trimer state for the same family of the He-He potentials presented in Table III of Ref. [47] (not shown), which gives  $E_* \approx 0.15$  mK at the unitary limit and reaffirms the robust universal property across different He-He potentials. Actually, based on the universal  $\kappa_*$  suggested in Ref. [17] for the van der Waals interactions, i.e.,

TABLE II. The numerically calculated three-body recombination rates in the zero-collision-energy limit and the extracted  $a_*$  based on the zero-range universal function Eq. (9) using these numerically calculated rates respectively as input.

Potential	$K_3$ (cm <sup>6</sup> /s)	$a_*$ (a.u.)	$a_*$ (Å)	Potential	$K_3$ (cm <sup>6</sup> /s)	$a_*$ (a.u.)	$a_*$ (Å)
B	$4.804 \times 10^{-28}$	148.254	78.453	Br.c.	$1.056 \times 10^{-27}$	149.513	79.119
BA	$2.816 \times 10^{-28}$	147.549	78.079	BAr.c.	$6.839 \times 10^{-28}$	148.743	78.712
BAR	$8.962 \times 10^{-28}$	149.275	78.993	BARr.c.	$8.137 \times 10^{-28}$	149.097	78.899
BARQ	$7.769 \times 10^{-28}$	149.009	78.852	BARQr.c.	$7.944 \times 10^{-28}$	149.070	78.884
LM2M2	$3.084 \times 10^{-27}$	151.724	80.289	HFD-B3-FCI1	$8.800 \times 10^{-28}$	149.277	78.994

$\kappa_* = 0.226e^{-\pi/s_0}/r_{\text{vdW}}$  [48], and the  $r_{\text{vdW}}$  of our reconstructed He-He potentials shown in Table I, it is easy to get  $\kappa_* = 1.960 \times 10^{-3}$  a.u. for the  $^4\text{He}_3$  system, which agrees within 3% with our fitted result and again confirms the universality of  $\kappa_*$  or the so-called van der Waals universality.

Inserting the fitted  $\kappa_*$  and  $\Gamma$  in Eq. (10) and equating the variable of  $\sin^2$  to zero, we get  $a_* = 144.247$  a.u., which is expected to be more accurate than those extracted based on Eq. (9) because of the correct inclusion of the finite-range effects. Here, the unique  $a_*$  obtained above is also the manifestation of the van der Waals universality. In fact, in the study of the van der Waals universality for the systems with positive  $a$ , it is found that  $a_*$  is around  $27.7r_{\text{vdW}}$  [27]. Using the  $r_{\text{vdW}}$  of our reconstructed He-He potentials shown in Table I, it gives  $a_* \approx 140.744$  a.u. for the  $^4\text{He}_3$  system, which differs by only 2% from ours. Based on our fitted  $a_*$  and the numerically determined relation between  $a_*$  and  $a_-$  in Ref. [27], i.e.,  $a_*/a_- = -0.143 \times 19.7 = -2.817$  [48], it is found that  $a_- = -10.08r_{\text{vdW}}$ , which only differs by about 3% from the suggested universal result  $-9.73r_{\text{vdW}}$  in Ref. [17] (see also Refs. [17,27] for relevant discussions and comparisons of their results with the experimental data). Therefore, the perfect fit of Eq. (10) to our numerical results indeed indicates a robust manifestation of the van der Waals universality.

Of course, as described before, besides the modifications used in Eq. (10), an adaptive  $a_*$  in Eq. (9) could be also introduced directly to encapsulate the finite-range effects. Particularly, when the short-range physics is non-negligible in the TBR process, a variational  $a_*$  may be extracted using Eq. (9). To investigate the possible variational behavior of  $a_*$  or the dependence of  $a_*$  on the short-range physics, each numerically accurate TBR rate calculated in the present paper is respectively used as input in Eq. (9) to extract  $a_*$  and the results as well as these calculated TBR rates are shown in Table II. Figure 3 shows the variation of  $1/a_*$  as a function of  $1/a$  for the  $^4\text{He}_3$  system (symbols). Interestingly, it is found that there is nearly a linear relation between them.

To understand such a variational behavior, the zero-range universal function Eq. (9) should be reassessed. If  $a_*$  is replaced by  $\kappa_*$  through the relation  $a_* = e^{-1.16/s_0}/\kappa_*$ , the variable of  $\sin^2$  and  $\cos^2$  in Eq. (9) becomes  $s_0 \ln(a/\kappa_*) + 1.16$ , i.e.,

$$s_0 \ln(a/a_*) = s_0 \ln(a/\kappa_*) + 1.16. \quad (11)$$

In order to take into account the finite-range effects, the TBP  $\kappa_*$  in Eq. (11) should be replaced by  $\kappa_* + \Gamma/a$ , which is one important substitution in deriving Eq. (10) based on the zero-range universal function [33,46] and theoretically justified by

the running Efimov parameter proposed by Ji *et al.* [26]. Then, we have that

$$s_0 \ln(a/a_*) = s_0 \ln(a\kappa_* + \Gamma) + 1.16. \quad (12)$$

From the above equation, the variation of  $1/a_*$  versus  $1/a$  can be deduced:

$$\frac{1}{a_*} = e^{1.16/s_0} \left( \kappa_* + \frac{\Gamma}{a} \right) = A_1 + A_2 \frac{1}{a}. \quad (13)$$

We have a linear relation between  $1/a_*$  and  $1/a$ , which could be used to describe the linearly variational behavior of  $1/a_*$  versus  $1/a$  shown in Fig. 3. To account for this, we perform the fit using the data associated with the reconstructed He-He potentials (see Tables I and II) and the result is shown as the black dashed line in Fig. 3. As can be seen, this linear fit agrees very well with all the numerically calculated data. Inserting the fitted values of  $A_1 = 5.518 \times 10^{-3}$  and  $A_2 = 2.035 \times 10^{-1}$  into Eq. (13), we find that  $\kappa_* = 1.742 \times 10^{-3}$  a.u. and  $\Gamma = 6.425 \times 10^{-2}$  a.u., which are comparable to the fitted values based on Eq. (10). To be exact, these two separately fitted values of  $\kappa_*$  agree within 10%, while the difference between the two fitted values of  $\Gamma$  is a little larger (roughly 36%). We consider this to be in reasonable agreement because another replacement of  $a$  by  $a_B$  in the zero-range universal function is also used in deriving Eq. (10). Actually,

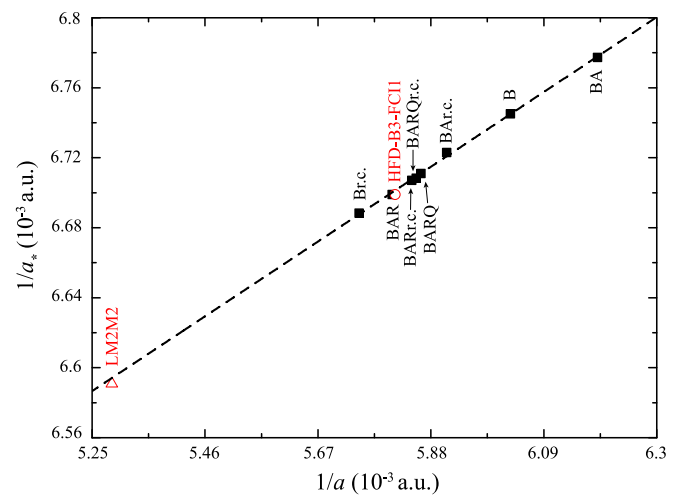


FIG. 3. The inverse of the three-body parameter ( $1/a_*$ ) as a function of the inverse of the scattering length ( $1/a$ ).  $a_*$  is extracted from the zero-range universal function Eq. (9) using the numerically calculated  $K_3$  as input. The black dashed line is a linear fit to the data associated with the filled squares based on Eq. (13), which gives  $A_1 = 5.518 \times 10^{-3}$  and  $A_2 = 2.035 \times 10^{-1}$ .

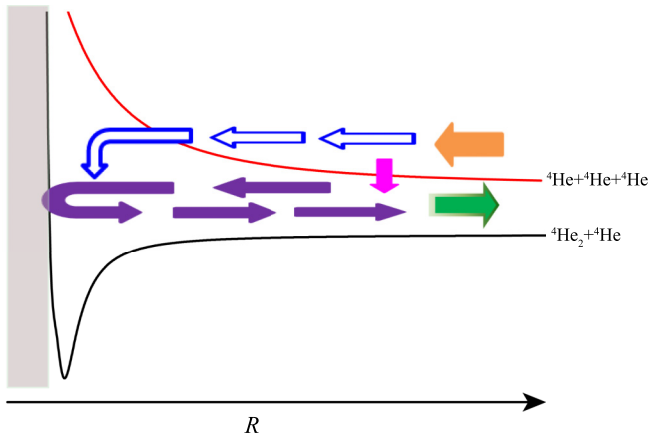


FIG. 4. Schematic diagram of the major reaction pathways mentioned in the main text. The shadow area denotes the classically forbidden region.

the fitted  $\kappa_*$  of this model, i.e., Eq. (13), differs by only 11% from the suggested  $\kappa_*$  in Ref. [17] and is well located within the stated 15% margin.

Inserting the fitted  $\kappa_*$  and  $\Gamma$  into the right side of Eq. (12) and equaling it to zero, we could also extract the TBP  $a_*$ , which gives  $a_* = 144.374$  a.u. This value agrees very well with that extracted based on Eq. (10), which can be ascribed to the fact that both models could make accurate predictions of the numerical TBR rates, comparing the black dashed curve and symbols in Fig. 2. In addition, it should be noted that a more accurate analysis shows that the empirical parameter  $\Gamma$ , considered as a constant fitting parameter in the two models discussed before, depends also slowly on  $\kappa_*$  (see Refs. [26,46] for relevant discussions).

According to the analysis before, either the modifications of the zero-range universal function used in Eq. (10) or the variation of  $a_*$  when extracted based on Eq. (9) undoubtedly indicates the non-negligible effect of the finite-range corrections or the short-range physics. Particularly, the linearly variational behavior of  $1/a_*$  versus  $1/a$  shown in Fig. 3 clearly indicates that the role of the short-range physics in the TBR process tends to be more and more important with the decrease of  $a$ . To understand the underlying mechanism, the two well-known interference pathways of the flow in the lowest two effective potentials are sketched in Fig. 4 (see the filled arrows). Generally speaking, the flow in the lowest incident channel recombines into the Efimov channel near  $R \approx a$  (see the filled purple arrow). Then, the system continues to decrease its size and the preformed molecule rebounds off the third atom near the classical turning point (see the filled blue arrows). This flow pathway will interfere with the original recombination pathway denoted by the purple arrow and consequently influences the formation of the molecular products (see the filled green arrow). In the zero-range limit, the destructive interference occurs in the TBR process when the variable of  $\sin^2$  in Eq. (9) is equal to zero. For the present  ${}^4\text{He}_3$  system, the unique recombination channel corresponds to the Efimov channel. In addition, because the scattering length of the He-He interaction is roughly equal to  $a_*$ , the

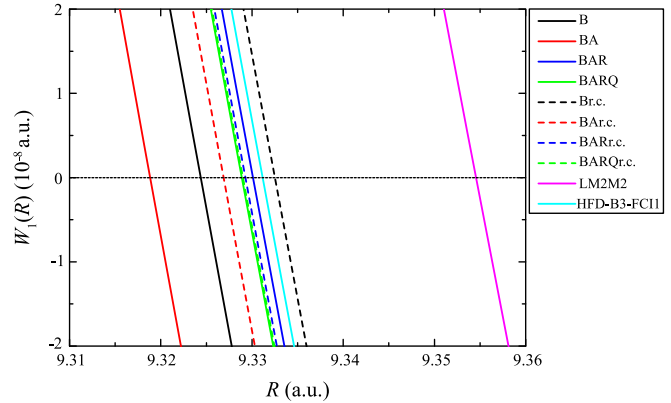


FIG. 5. For the zero-collision-energy limit, a zoom-in plot of the classical turning points of the flow governed by the Efimov channel for all the considered cases (see the main text). The horizontal dashed line denotes the zero-collision-energy limit.

relevant TBR process is near one of these destructive interferences.

The universality of the TBP  $a_-$  is ascribed to the converged potential wall near  $R \approx 2r_{\text{vdW}}$  in the Efimov channel [17], which prevents the reactants from getting much closer to experience the short-range interactions. Here, in contrast, the effects of the short-range physics on the scattering process should be also related to the variation of the potential wall in the small- $R$  region, which modifies the flow pathway in the Efimov channel (see the pathway denoted by the filled blue arrows in Fig. 4). Figure 5 shows the potential walls associated with the Efimov channel for all the present cases. Note that the classical turning point of the probability flow in the Efimov channel for each case, which characterizes to some extent the position of the potential wall, is denoted by the crossing of the corresponding potential wall and the horizontal dashed line at  $E \rightarrow 0$ . As displayed, these classical turning points are also roughly  $2r_{\text{vdW}}$  (see also Table I for  $r_{\text{vdW}}$  of the interacting pair for these cases), but there exists a small variation.

Actually, except for a small departure for the case calculated using the HFD-B3-FC11 He-He potential, the classical turning point is nearly proportional to the corresponding scattering length of the He-He potential. Therefore, with the decrease of  $a$ , the flow in the Efimov channel will take a longer travel time before interfering with the recombination pathway denoted by the filled purple arrow in Fig. 4, which leads to the departure of the realistic TBR process from the destructive interference predicted in the zero-range limit. Consequently, the realistic TBR rate is more and more underestimated by the zero-range universal function with the decrease of  $a$ . Therefore, the small variation of the potential wall near  $R \approx 2r_{\text{vdW}}$  in the Efimov channel is expected to, in large part, account for the linearly variational behavior of  $1/a_*$  versus  $1/a$  shown in Fig. 3. Here, it should be emphasized that the variation of the classical turning point in the Efimov channel is the result of the three-body interaction. There is no simple proportional relation between the variation of the two-body He-He interaction at a short internuclear distance and that of the classical turning point in the Efimov channel, comparing the inset of

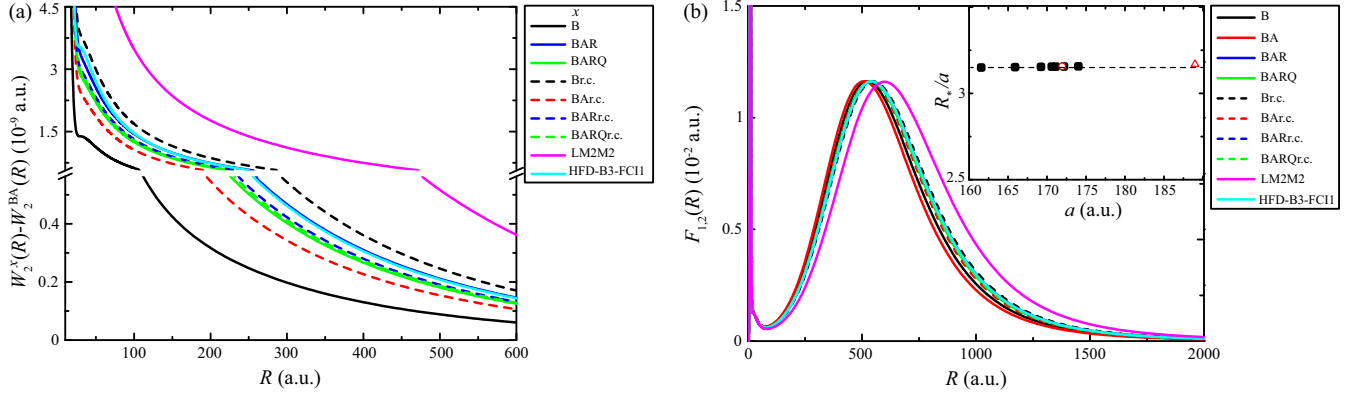


FIG. 6. (a) The differences of the lowest incident channels between the one where  $V(R; \theta, \varphi)$  is constructed by  $V_{BA}(r)$  and all the other cases. (b) The nonadiabatic coupling strength between the lowest incident and recombination channels, i.e.,  $F_{1,2}(R)$ , for all these cases considered in the main text. The inset displays the ratio of the hyperradius  $R_*$ , where  $F_{1,2}(R)$  peaks at relatively large  $R$ , to the corresponding scattering length. The dashed line shows the ratio value of 3.15.

Fig. 1(a) and Fig. 5, which is again the clear manifestation of the van der Waals universality.

In addition, the small departure of the case calculated by the HFD-B3-FCI1 He-He potential from others implies that there may exist other non-negligible short-range physics accounting for the linearly variational behavior of  $1/a_*$  versus  $1/a$  shown in Fig. 3. Note that the shape of the potential well for this case actually also has a small departure from others (not shown). The leading one of the other influence factors is that the flow in the lowest incident channel tunnels into the small- $R$  region and jumps into the Efimov channel at the small hyperradius where the peak of  $F_{1,2}(R)$  occurs (see the open blue arrows in Fig. 4). Here, since the effective potentials associated with the lowest incident channel for these cases are difficult to be directly distinguished, the differences between the case constructed using  $V_{BA}(r)$  and other cases are calculated and shown in Fig. 6(a). As shown, the lowest incident channel tends to be more and more repulsive with the increase of the scattering length of the He-He interaction. In other words, this signifies that the flow pathway indicated by the open blue arrows in Fig. 4 tends to be easier to occur with the decrease of  $a$ , which consequently leads to the increase of the TBR rate. To some extent, this clearly accounts for the departure of the numerically calculated TBR rates from the prediction of the zero-range universal function (see Fig. 2), or the corresponding linearly variational behavior of  $1/a_*$  versus  $1/a$  shown in Fig. 3.

To give an intuitive picture of the tunneling probability in the lowest incident channel for these cases, the position  $R_*$  of the recombination pathway near  $R \approx a$  (the filled purple arrow in Fig. 4), which can be characterized by the hump of the nonadiabatic coupling strength  $F_{1,2}(R)$  at relatively large  $R$ , is first located. Figure 6(b) shows  $F_{1,2}(R)$  for the present cases and the inset exhibits the value of  $R_*/a$ , which gives  $R_* \approx \lambda a$  with  $\lambda \approx 3.15$ . Note that the departure of  $R_*$  from  $a$  should be ascribed to the fact that the scattering length of the He-He potential is not anomalously large. In addition, replacing  $a$  by  $R_*$  directly has no effect on the prediction of the zero-range universal function. Therefore, to some extent, it is a possible flow pathway in the lowest incident channel

from  $R_*$  to the small- $R$  region (see the open blue arrows in Fig. 4), accounting for the departure of the zero-range universal prediction associated with the two interference pathways from the realistic TBR rates.

To characterize its effects on the TBR process of the  $^4\text{He}_3$  system, the WKB tunneling probability is used to evaluate the recombination probability associated with this flow pathway (see also the open blue arrows in Fig. 4):

$$P_{R_* \rightarrow R}^{v=2} = \exp \left[ -2 \int_R^{R_*} \sqrt{2\mu W_v(R)} dR \right]. \quad (14)$$

As shown in Fig. 7, the tunneling probability of the flow in the lowest incident channel is inversely proportional to its repulsive behavior shown in Fig. 6(a). As described before, with the decrease of the scattering length of the He-He potential, the flow in the lowest incident channel tends to be much easier to tunnel into the smaller hyperradial region and jumps into the Efimov channel. This may also account, to some extent, for the fact that the accurate TBR rate becomes larger than the zero-range universal prediction with the decrease of the scattering length of the He-He potential. Of course, as the next leading correction to the zero-range universal theory, it

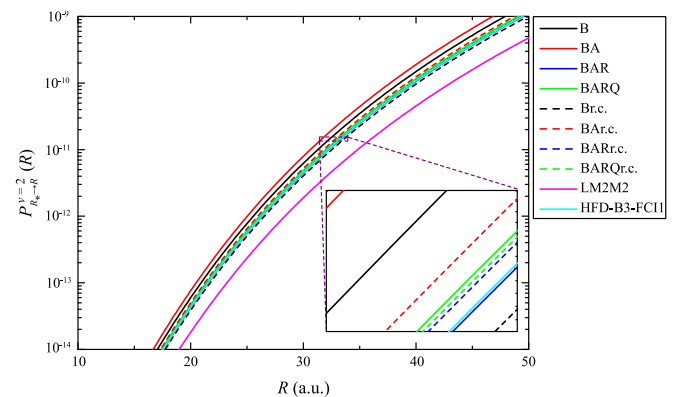


FIG. 7. For the zero-collision-energy limit, the tunneling probability of the incident flow in the lowest incident channel from  $R_*$  [see Fig. 6(b)] to the small  $R$ .



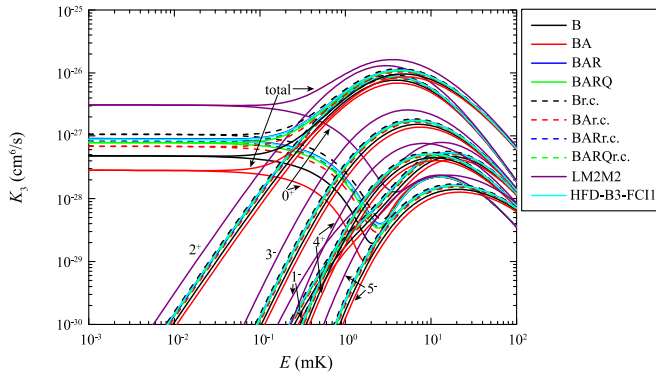


FIG. 8. The total and partial three-body recombination rates for all these cases considered in the main text.

is also expected to account for the small departure of the case calculated by the HFD-B3-FC11 He-He potential from other cases.

Finally, the post-BO effects on the TBR process of the  $^4\text{He}_3$  system for the partial wave with the total angular momentum  $J > 0$  are also calculated, which are shown in Fig. 8. As displayed, similar to those in the zero-collision-energy limit, the post-BO effects on the TBR rate are also proportional to the scattering length of the He-He potential for these partial waves before they gradually become indistinguishable with the increase of the collision energy  $E$ . For  $J^\Pi = 0^+$  symmetry with  $\Pi$  denoting the parity of the system, it is found that the depth of the Stückelberg minimum, the manifestation of the destructive interference between the two main recombination pathways described before in  $E$ , is also inversely proportional to the scattering length of the He-He potential. With the increase of  $a$ , the Stückelberg minimum becomes shallower and its position is shifted to larger  $E$ .

#### IV. CONCLUSION

In summary, based on various post-BO corrections on the standard BO He-He interaction and two widely adopted He-He potentials, the effects of the short-range physics on the

TBR process of the  $^4\text{He}_3$  system have been investigated. It is found that the numerically accurate TBR rates could be well predicted by the zero-range Efimov universal function when a linearly variational  $1/a_*$  versus  $1/a$  is introduced. Particularly, two leading short-range mechanisms are investigated to account for the variation of  $1/a_*$  versus  $1/a$ . One is associated with the flow in the Efimov channel at short hyperradial distances, which is characterized by the classical turning point. With the decrease of  $a$ , the flow in the Efimov channel will take a longer travel time to go through the short hyperradial distance before interfering with the other main recombination pathway, which consequently leads to the variation of the extracted  $a_*$ . The other one is associated with the short-range tunneling probability of the flow in the lowest incident channel, which is inversely proportional to  $a$ . So the tunneling probability is larger for a smaller  $a$ , which consequently leads to a larger TBR rate than that predicted by the zero-range universal function. In addition, a perfect fit of the modified universal function proposed by Garrido *et al.* [33] or the zero-range universal function with a linearly variational  $1/a_*$  versus  $1/a$  to our numerical data indicates a clear manifestation of the van der Waals universality. Finally, the post-BO effects on the TBR process for the partial wave with the total angular momentum  $J > 0$  are discussed and found to be also similar to those in the zero-collision-energy limit before they gradually become indistinguishable with the increase of the collision energy.

#### ACKNOWLEDGMENTS

This work is supported by the National Natural Science Foundation of China (Grant No. 22103063), Sichuan Science and Technology Program (Grant No. 2023NSFSC1368), and the Sichuan Youth Science and Technology Innovation Research Team (Grant No. 21CXTD0038). Y.-C.H. acknowledges support from the National Key Research and Development Program of China (Grant No. 2018YFA0306503) and the National Natural Science Foundation of China (Grant No. 12174044).

- [1] V. Efimov, *Phys. Lett. B* **33**, 563 (1970).
- [2] B. D. Esry, C. H. Greene, and J. P. Burke, *Phys. Rev. Lett.* **83**, 1751 (1999).
- [3] E. Nielsen and J. H. Macek, *Phys. Rev. Lett.* **83**, 1566 (1999).
- [4] P. F. Bedaque, E. Braaten, and H.-W. Hammer, *Phys. Rev. Lett.* **85**, 908 (2000).
- [5] E. Braaten and H.-W. Hammer, *Phys. Rep.* **428**, 259 (2006).
- [6] T. Kraemer, M. Mark, P. Waldburger, J. G. Danzl, C. Chin, B. Engeser, A. D. Lange, K. Pilch, A. Jaakkola, H.-C. Nägerl, and R. Grimm, *Nature (London)* **440**, 315 (2006).
- [7] J. Ulmanis, S. Häfner, E. D. Kuhnle, and M. Weidemüller, *Nat. Sci. Rev.* **3**, 174 (2016).
- [8] P. Naidon and S. Endo, *Rep. Prog. Phys.* **80**, 056001 (2017).
- [9] C. H. Greene, P. Giannakeas, and J. Pérez-Ríos, *Rev. Mod. Phys.* **89**, 035006 (2017).
- [10] J. P. D’Incao, *J. Phys. B* **51**, 043001 (2018).
- [11] Y. Nishida, Y. Kato, and C. D. Batista, *Nat. Phys.* **9**, 93 (2013).
- [12] J. P. D’Incao, C. H. Greene, and B. D. Esry, *J. Phys. B* **42**, 044016 (2009).
- [13] M. Berninger, A. Zenesini, B. Huang, W. Harm, H.-C. Nägerl, F. Ferlaino, R. Grimm, P. S. Julienne, and J. M. Hutson, *Phys. Rev. Lett.* **107**, 120401 (2011).
- [14] S. Knoop, J. S. Borbely, W. Vassen, and S. J. J. M. F. Kokkelmans, *Phys. Rev. A* **86**, 062705 (2012).
- [15] N. Gross, Z. Shotan, O. Machtay, S. Kokkelmans, and L. Khaykovich, *C. R. Phys.* **12**, 4 (2011).
- [16] C. Chin, *arXiv:1111.1484*.
- [17] J. Wang, J. P. D’Incao, B. D. Esry, and C. H. Greene, *Phys. Rev. Lett.* **108**, 263001 (2012).
- [18] P. Naidon, S. Endo, and M. Ueda, *Phys. Rev. A* **90**, 022106 (2014).

- [19] T. K. Lim, S. K. Duffy, and W. C. Damert, *Phys. Rev. Lett.* **38**, 341 (1977).
- [20] R. Brühl, A. Kalinin, O. Kornilov, J. P. Toennies, G. C. Hegerfeldt, and M. Stoll, *Phys. Rev. Lett.* **95**, 063002 (2005).
- [21] E. A. Kolganova, A. K. Motovilov, and W. Sandhas, *Few-Body Syst.* **58**, 35 (2017).
- [22] E. Braaten and H.-W. Hammer, *Phys. Rev. A* **67**, 042706 (2003).
- [23] M. Kunitski, S. Zeller, J. Voigtsberger, A. Kalinin, L. P. H. Schmidt, M. Schoffler, A. Czasch, and W. Schollkopf, *Science* **348**, 551 (2015).
- [24] A. Kievsky, M. Gattobigio, L. Girlanda, and M. Viviani, *Annu. Rev. Nucl. Part. Sci.* **71**, 465 (2021).
- [25] M. Zaccanti, B. Deissler, C. D’Errico, M. Fattori, M. Jonas-Lasinio, S. Müller, G. Roati, M. Inguscio, and G. Modugno, *Nat. Phys.* **5**, 586 (2009).
- [26] C. Ji, E. Braaten, D. R. Phillips, and L. Platter, *Phys. Rev. A* **92**, 030702(R) (2015).
- [27] P. M. A. Mestrom, J. Wang, C. H. Greene, and J. P. D’Incao, *Phys. Rev. A* **95**, 032707 (2017).
- [28] R. Chapurin, X. Xie, M. J. Van de Graaff, J. S. Popowski, J. P. D’Incao, P. S. Julienne, J. Ye, and E. A. Cornell, *Phys. Rev. Lett.* **123**, 233402 (2019).
- [29] Y. Wang and P. S. Julienne, *Nat. Phys.* **10**, 768 (2014).
- [30] K.-M. Tempest and S. Jonsell, *Phys. Rev. A* **107**, 053319 (2023).
- [31] E. Braaten, D. Kang, and L. Platter, *Phys. Rev. A* **75**, 052714 (2007).
- [32] J. R. Shepard, *Phys. Rev. A* **75**, 062713 (2007).
- [33] E. Garrido, M. Gattobigio, and A. Kievsky, *Phys. Rev. A* **88**, 032701 (2013).
- [34] M. Przybytek, W. Cencek, J. Komasa, G. Lach, B. Jeziorski, and K. Szalewicz, *Phys. Rev. Lett.* **104**, 183003 (2010).
- [35] W. Cencek, M. Przybytek, J. Komasa, J. B. Mehl, B. Jeziorski, and K. Szalewicz, *J. Chem. Phys.* **136**, 224303 (2012).
- [36] B.-B. Wang, S.-H. Jing, and T.-X. Zeng, *J. Chem. Phys.* **150**, 094301 (2019).
- [37] H. Suno, B. D. Esry, C. H. Greene, and J. P. Burke, *Phys. Rev. A* **65**, 042725 (2002).
- [38] H. Suno and B. D. Esry, *Phys. Rev. A* **78**, 062701 (2008).
- [39] J. C. Light, R. B. Walker, E. B. Stechel, and T. G. Schmalz, *Comput. Phys. Commun.* **17**, 89 (1979).
- [40] H. B. G. Casimir and D. Polder, *Phys. Rev.* **73**, 360 (1948).
- [41] R. A. Aziz and M. J. Slaman, *J. Chem. Phys.* **94**, 8047 (1991).
- [42] R. A. Aziz, A. R. Janzen, and M. R. Moldover, *Phys. Rev. Lett.* **74**, 1586 (1995).
- [43] C. Chin, R. Grimm, P. Julienne, and E. Tiesinga, *Rev. Mod. Phys.* **82**, 1225 (2010).
- [44] The present function is six times larger than theirs due to different definitions of the TBR rate.
- [45] A. Kievsky, A. Polls, B. Juliá-Díaz, N. K. Timofeyuk, and M. Gattobigio, *Phys. Rev. A* **102**, 063320 (2020).
- [46] A. Kievsky and M. Gattobigio, *Phys. Rev. A* **87**, 052719 (2013).
- [47] E. Hiyama and M. Kamimura, *Phys. Rev. A* **85**, 062505 (2012).
- [48]  $\kappa_*$  given in Ref. [17] and the ratios between different TBPs calculated in Ref. [27] should be applied to the  $^4\text{He}_3$  system, the extracted  $\kappa_*$  and  $a^*$  of which are associated with the first excited Efimov state in this paper.